GNSS Inter-User Ranging for Lunar Orbiters Flying the Spaceborne Navimoon Receiver

GNSS inter-user ranging for lunar orbiters flying the spaceborne NaviMoon receiver

Anaïs Delépaut
Dept. of Electronics and Telecommunications (DET)
Politecnico di Torino
Turin, Italy
anais.delepaut@polito.it

Alex Minetto
DET
Politecnico di Torino
Turin, Italy
alex.minetto@polito.it

Pietro Giordano
ESTEC
European Space Agency
Noordwijk, Netherlands
pietro.giordano@esa.int

Fabio Dovis
DET
Politecnico di Torino
Turin, Italy
fabio.dovis@polito.it

***Abstract*—In 2024, a pivotal moment in space navigation occurs as a GNSS receiver journeys to the Moon, marking its inaugural lunar deployment to showcase GNSS navigation feasibility at lunar altitudes. However, the challenge of increasing Dilution Of Precision with greater distance from GNSS constellations remains a significant barrier to the effective use of GNSS in space. Consequently, achieving the requisite accuracy for reliable autonomous GNSS navigation at lunar distances is uncertain. As an enabler of potential collaborative navigation paradigms relying on GNSS measurements, this study proposes a GNSS-based inter-user baseline estimation technique, previously effective in terrestrial scenarios, and analyzes different methodologies to achieve unbiased baseline estimation in space navigation. This solution primarily benefits from the fact that it is non-invasive and solely based on the availability of a communication link between the cooperating space users. The present work shows the application of the estimation of the baseline length between a lunar CubeSat mission, VMMO, and the communication relay Lunar Pathfinder mission. Most notably, this is performed using real GNSS measurements generated by an actual Engineering Model of the NaviMoon receiver in the ESA/ESTEC Radio Navigation Laboratory, while being fed by GNSS signals emulated by a radio-frequency constellation simulator.**

***Index Terms*—ranging in space, GNSS, lunar missions**

I. Introduction

Given the momentum taken by the space sector for lunar exploration both by private and governmental actors, scientific and commercial initiatives are expected to expand in the 2020s, led by European Space Agency (ESA)'s Moonlight initiative and NASA's Artemis program [1]. Therefore, the development of guidance, navigation, and control solutions being independent of tracking and controlling ground segments is strongly desired for lunar exploration. In particular, the south pole region of the Moon is attracting attention from the perspective of human activity bases and exploration. In this context, ESA and the National Aeronautics and Space Administration (NASA) together with the Italian Space Agency (ASI) will fly In-Orbit demonstration missions around the Moon with, respectively, the Surrey Satellite Technology Ltd (SSTL) Lunar Pathfinder flying the NaviMoon receiver in 2025 and the Firefly Blue Ghost Mission 1 flying a multiconstellation Global Navigation Satellite System (GNSS) receiver payload in 2024 in the framework of the Lunar GNSS Receiver Experiment (LuGRE) [2], [3]. Both will track Galileo E1, E5a, and GPS L1 C/A, L5 signals, and will return pseudorange, carrier phase and Doppler measurements.

In the field of terrestrial GNSS applications, Differential GNSS (DGNSS)-Cooperative Positioning (CP) has been proven successful in leveraging the presence of neighbouring GNSS users as anchors of opportunities by relying on inter-users or relayed communication links to improve the positioning performances of each user individually [4]. This technology has already proven useful in terrestrial scenarios involving bad GNSS visibility, such as collaborative vehicle networks and mobile users [5], [6]. The basic idea behind DGNSS-CP is to measure the relative distance between GNSS users by exchanging information about their respective pseudoranges to a common set of tracked GNSS satellites. More specifically, a user with poor GNSS visibility can share raw GNSS measurements through a communication link with another user (auxiliary agent) to estimate their baseline vector. Subsequently, this relative distance is used in the Position Velocity Time (PVT) solution estimation using a Weighted Least Squares estimation applied to Double Differences (DD)s between the observed pseudoranges, thus removing both satellites and receiver clock bias. Even when it is noisy and correlated to the other GNSS range measurements, this additional ranging information was proven to be beneficial in low visibility and high Dilution of Precision (DOP) scenarios [6].

The present research focuses on assessing the use of these GNSS-based relative ranging techniques to a space scenario, discussing the applicability of the method when compared to a terrestrial case. The implementation of such a paradigm for space would offer a non-invasive ranging solution. In fact, cooperating spacecrafts would be able to use it also when they are not in Line-of-Sight (LoS) leveraging on a relayed communication link. Furthermore, it could also contribute to improve the geometric distribution of ranging sources. Along with the remarkable research effort paid towards the use of GNSS in space, relative GNSS navigation, as well, has attracted a number of scientific contributions. Advanced algorithms have been designed that leverage carrier-phase measurements and integer ambiguity resolution to support formation-flying Low-Earth Orbit (LEO) satellites, such as the NASA's GRACE and ESA's TanDEM-X missions [7]. More

979-8-3503-8078-1/24/$31.00

recently, works addressed the relative LEO navigation problem for rendez-vous and docking within distances within 10 km [8], and extending this range up to 60–175 km in [9]. However, fundamental GNSS ranging techniques investigated in this work may still represent a valuable and lower-complexity alternative.

In the present contribution, the results are obtained making use of GNSS observables generated by a GNSS receiver specifically designed for a Moon mission. The Moon receiver is called the NaviMoon and will be hosted by the Lunar Pathfinder space mission [10].

The paper is structured as follows: Section II describes the fundamentals of the GNSS-based baseline estimation, Section III describes the limitations of terrestrial algorithms applied to space scenarios and proposes specific modifications to achieve unbiased baseline estimation. Section IV describes the considered space scenario and its GNSS visibility characteristics. Section V describes the functional blocks of the test bench designed to analyze the performances of the presented techniques on the ESA/SpacePNT's NaviMoon receiver. Finally, VI presents the results achieved with this environment and analyzes the potential performances of inter-agent GNSS ranging in space.

II. GNSS INTER-AGENT RANGING

By considering a pair of moving agents (i.e. spacecrafts) i and j, at a given time instant t_k, relative ranging technologies allow to estimate their *inter-agent distance* (a.k.a. *baseline length*)

$$d_{ij,k} = ||\mathbf{d}_{ij,k}|| = ||\mathbf{x}_{j,k} - \mathbf{x}_{i,k}|| \tag{1}$$

where the operator $||\cdot||$ is the Euclidean norm and $\mathbf{x}_{i,k}$, $\mathbf{x}_{j,k}$ are the actual locations of the agents in a given Cartesian reference frame. While radio-frequency ranging solutions directly provide an estimate of (1) by means of signal Time of Flight (ToF) or Round Trip Time (RTT), DGNSS techniques first estimate a displacement vector, a.k.a. *baseline vector*

$$\mathbf{d}_{ij,k} = \begin{bmatrix} \Delta x_{ij,k} & \Delta y_{ij,k} & \Delta z_{ij,k} \end{bmatrix}. \tag{2}$$

Through DGNSS techniques, the inter-agent distance estimation can be obtained by applying the Euclidean norm to an estimate of (2), namely $\hat{\mathbf{d}}_{ij,k}$. The DGNSS estimation of inter-agent distances is achieved through few differential methods [4], based on the combination of pseudorange measurements from independent, networked GNSS receivers, following the exchange of this data from one agent, defined as the *aiding agent*, to another, the *aided agent*, as depicted in Fig. 1a. Different algorithms can be selected according to their capability of canceling all the systematic biases (i.e., receiver and satellites clock biases) [11], at the cost of an increased output variance [12]. Despite the fact that ionospheric and troposheric errors can be reasonably neglected at lunar distances, other unmodelled, common sources of error may affect the spaceborne receivers and could be effectively compensated through these techniques. Therefore, the present section presents all the GNSS ranging techniques that the present contribution applied to a lunar scenario of DGNSS.

1) Absolute Positions Differencing (APD): The first technique presented in this paper is called Absolute Positions Differencing and is based on taking the Euclidean norm of the difference of the Single Point Position (SPP) estimations of each user individually, as per (3).

$$\hat{d}_{ij,k} = ||\hat{\mathbf{d}}_{ij,k}|| = ||\hat{\mathbf{x}}_{j,k} - \hat{\mathbf{x}}_{i,k}|| \tag{3}$$

Hence, in this technique, the exchange of the SPP position estimate from the aiding agent to the aided agent is considered. The SPP estimate of each user is obtained thanks to an Iterative Least Squares (ILS) estimator, where at each iteration l, the user assumed position $\hat{\mathbf{x}}_{*,k}$ is updated based on the linearisation of the pseudorange equation with a Taylor expansion truncated at the first order:

$$\hat{\mathbf{x}}_{*,k} = \hat{\mathbf{x}}^{l-1}_{*,k} + \Delta\hat{\mathbf{x}}^{l}_{*,k} \tag{4}$$

where $\hat{\mathbf{x}}^{l-1}_{*,k}$ is the position estimated at the previous iteration for user $*$ (i or j, interchangeably) and $\Delta\hat{\mathbf{x}}^{l}_{*,k}$ is the increment in position for the current iteration l and is obtained together with the user clock bias increment $\Delta\hat{b}^{l}_{*,k}$ with:

$$\begin{bmatrix} \Delta\hat{\mathbf{x}}^{l}_{*,k} \\ \Delta\hat{b}^{l}_{*,k} \end{bmatrix} = \left(\mathbf{H}^\top\mathbf{H}\right)^{-1}\mathbf{H}^\top\boldsymbol{\Delta\rho}^{l}_{*,k}, \tag{5}$$

where $\mathbf{H}$ is the $N \times 4$ direction cosine matrix estimated from the most recent estimation of the user position and is made of the *unit steering vector* to the satellites, $\mathbf{h}^*_*$, [13]. $\boldsymbol{\Delta\rho}^{l}_{*,k}$ is the pseudorange increment vector $N \times 1$ which has been corrected for the user clock bias and the Signal In Space Error (SISE) as well as the relativistic effects. N represents the number of GNSS satellites involved in the computation and must be at least equal to 4.

2) Pseudorange Ranging: This method computes the *baseline vector* by differencing the position estimates of both users obtained via a joint estimation process around a common linearisation point. This is achieved by expressing the position of the aiding agent as a function of the aided agent's position and the baseline vector for each time instant k:

$$\mathbf{x}_{j,k} = \mathbf{x}_{i,k} + \mathbf{d}_{ij,k} \tag{6}$$

In this case, (5) becomes:

$$\begin{bmatrix} \Delta\hat{\mathbf{x}}^{l}_{i,k} \\ \Delta\hat{b}^{l}_{i,k} \\ \Delta\hat{\mathbf{x}}^{l}_{j,k} \\ \Delta\hat{b}^{l}_{j,k} \end{bmatrix} = \left(\mathbf{H}^\top_{PR}\mathbf{H}_{PR}\right)^{-1}\mathbf{H}^\top_{PR}\boldsymbol{\Delta\rho}^{l}_{ij,k}, \tag{7}$$

where $\mathbf{H}_{PR}$ is

$$\mathbf{H}_{PR} = \begin{bmatrix} \mathbf{H} & 0_{N\times 4} \\ 0_{N\times 4} & \mathbf{H} \end{bmatrix}, \tag{8}$$

and $\boldsymbol{\Delta\rho}^{l}_{ij,k}$ is the apposition of the pseudorange increments from user i and user j in a $2N \times 1$ vector, after correction of their respective previously estimated clock bias $\hat{b}^{l-1}_{*,k}$.

3) Single Differences Ranging: Also based on the exchange of the pseudorange measurements from the aiding to the aided agent, this technique exploits a set of differential quantities known as Single Differences (SD). A generic SD can be defined between two GNSS receivers, i and j tracking a common satellite s as the difference between synchronous pseudorange measurements:

$$\begin{aligned} S^s_{ij,k} &= \rho^s_{j,k} - \rho^s_{i,k} \\ &= \Delta r^s_{ij,k} + \Delta b_{ij,k} + \Delta \epsilon_{ij,k}, \end{aligned} \tag{9}$$

where $\Delta b_{ij,k}$ is the difference between the clock biases of the two agents and $\Delta \epsilon_{ij,k}$ is a noise term which aggregates all the non-correlated errors. In fact, provided that all the measurements are synchronous, SDs allow to cancel the satellite clock bias and correlated bias terms affecting pseudorange measurements. Besides the cancellation of correlated error terms, the variance of the uncorrelated errors, such as thermal noise, is increased. These noise contributions are hence aggregated in $\Delta \epsilon_{ij,k}$.

The computation of the baseline vector based on SD is performed through (10), assuming a minimum of 4 visible GNSS satellites common to both users.

$$\begin{bmatrix} S^1_{ij,k} \\ S^2_{ij,k} \\ \vdots \\ S^S_{ij,k} \end{bmatrix} \simeq - \begin{bmatrix} \mathbf{h}^1_{i,k} & 1 \\ \mathbf{h}^2_{i,k} & 1 \\ \vdots & \vdots \\ \mathbf{h}^S_{i,k} & 1 \end{bmatrix} \begin{bmatrix} \mathbf{d}_{ij,k} \\ \Delta b_{ij,k} \end{bmatrix} \tag{10}$$

4) Double Differences Ranging: When the same pair of satellites r and s is visible to both receivers, a DD measurement can be obtained as difference of two SDs:

$$D^{sr}_{ij,k} = S^s_{ij,k} - S^r_{ij,k} = \Delta R^{sr}_{ij,k} + \Sigma_{ij,k}, \tag{11}$$

where S^s_{ij} is a SD computed according to (9) while Σ_{ij} is a random variable collecting residual error contributions that cannot be cancelled due to the non-correlation between the measurements such as multipath, second-order noise components of the receiver front-ends and residual, unmodelled noise contributions [13]. The term ΔR^{sr} can be expressed highlighting the dependency from the baseline vector as:

$$\Delta R^{sr,k} = \left[\mathbf{h}^r_{*,k} - \mathbf{h}^s_{*,k}\right]^T \mathbf{d}_{ij,k}. \tag{12}$$

In order to determine the steering vectors, an approximation of the two positions is needed. A GNSS receiver can solve for the aiding position by using the external pseudorange measurements. By means of this approach the exchange of the estimated position is not necessary since it can be computed autonomously at the aided receiver.

In the following, the inter-agent distance will be referred to as Inter-Spacecraft Range (ISR).

III. The potential of the DGNSS algorithm for space users using Earth navigation satellites

A. Parallelism assumption used for terrestrial applications

The performances of DGNSS in space are subject to variations with respect to the performances presented for terrestrial applications. This is due to the assumption taken to establish the relationship presented in (10). Indeed, as stated in [14] and [4], the system of equations presented in (10) comes from the assumption that the difference in true ranges $\Delta r^s_{ij,k}$ can be approximated by the inner product between the baseline vector $\mathbf{d}_{ij,k}$ and the unit steering vector $\mathbf{h}^s_{i,k}$ or $\mathbf{h}^s_{j,k}$ between either user i or j and the satellite s.

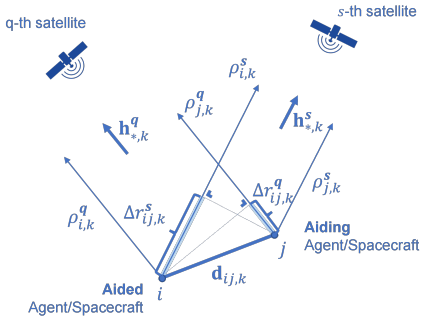

(a) *Valid assumption.*

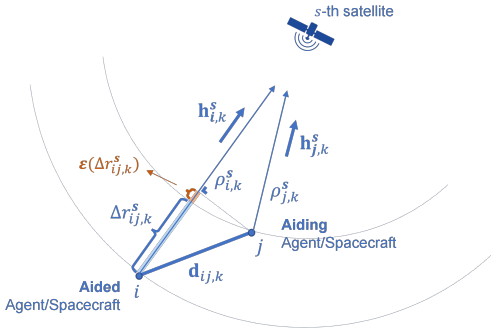

(b) *Invalid assumption.*

Fig. 1: *Assumption of parallelism within the DGNSS algorithm.*

$$\Delta r^s_{ij,k} \approx - \left[\mathbf{h}^s_{*,k}\right]^T \mathbf{d}_{ij,k} \tag{13}$$

This assumption holds while the true ranges $r^s_{i,k}$ and $r^s_{j,k}$ from satellite s to users i and j are much larger than the distance $d_{ij,k}$ between i and j, where in such a case their respective unit steering vector $\mathbf{h}^s_{i,k}$ and $\mathbf{h}^s_{j,k}$ are nearly parallel to each other, as depicted in Fig. 1a. However, the typical distances of a DGNSS scenario for spaceborne users are easily two orders of magnitudes larger than for terrestrial applications. Hence, this parallelism assumption is likely to introduce a bias in the ISR estimation process.

B. Bias introduced in case of parallelism assumption invalidity

As depicted in Fig. 1, when the distance between the users and the navigation satellites is not large enough with respect to the baseline length for the unit steering vectors originating from both users to be considered as parallel, a bias term $\varepsilon(\Delta r^s_{ij,k})$ is introduced:

$$\Delta r^s_{ij,k} = - \left[\mathbf{h}^s_{*,k}\right]^T \mathbf{d}_{ij,k} + \varepsilon_*(\Delta r^s_{ij,k}), \tag{14}$$

where, if the unit steering vectors from the aided agent $\mathbf{h}^s_{i,k}$ are used in the SD Least Squares (LS) $\mathbf{H}$ design matrix, the bias term can be written as

$$\begin{aligned}\varepsilon_i(\Delta r^s_{ij,k}) &= r^s_{i,k} - r^s_{j,k}\left[\mathbf{h}^s_{j,k}\right]^T\left[\mathbf{h}^s_{i,k}\right] + \Delta r^s_{ij,k} \\ &= r^s_{j,k} - r^s_{j,k}\left[\mathbf{h}^s_{j,k}\right]^T\left[\mathbf{h}^s_{i,k}\right] \\ &= r^s_{j,k}(1 - \left[\mathbf{h}^s_{j,k}\right]^T\left[\mathbf{h}^s_{i,k}\right]).\end{aligned} \tag{15}$$

C. Redefinition of the unit steering vectors for the space scenario

The proposed solution, that takes into account the invalidity of the parallelism assumption for space scenarios, while keeping the algorithm linear for its low-complexity advantage, is to redefine the unit vectors considered in the design matrix $\mathbf{H}$ from (10). Instead of using $\mathbf{h}^s_{i,k}$ or $\mathbf{h}^s_{j,k}$, the normalized sum of both will be used.

$$\mathbf{h}^s_{i+j,k} = \frac{\mathbf{h}^s_{i,k} + \mathbf{h}^s_{j,k}}{||\mathbf{h}^s_{i,k} + \mathbf{h}^s_{j,k}||} \tag{16}$$

Consequently, the difference in true ranges changes with respect to (13) and it becomes:

$$\Delta r^s_{ij,k} \approx -\left[\mathbf{h}^s_{i+j,k}\right]^T \mathbf{d}_{ij,k}. \tag{17}$$

Another solution presented in the literature in the context of differential Doppler positioning in [15], consists in finding the unit steering vector $\mathbf{h}^s_{ideal,k}$, which at each epoch k will satisfy exactly (13), such that:

$$\Delta r^s_{ij,k} = -\left[\mathbf{h}^s_{ideal,k}\right]^T \mathbf{d}_{ij,k}. \tag{18}$$

The angle θ_k between $\mathbf{h}^s_{ideal,k}$ and $\mathbf{d}_{ij,k}$ is given by:

$$\cos(\theta_k) = -\frac{\Delta r^s_{ij,k}}{d_{ij,k}}, \tag{19}$$

where $\mathbf{h}^s_{ideal,k}$ satisfying this condition form a conical surface. A solution consists in defining the vector $\mathbf{h}^s_{normal,k}$ normal to both $\mathbf{d}_{ij,k}$ and $\mathbf{h}^s_{i,k}$:

$$\mathbf{h}^s_{normal,k} = \frac{\mathbf{h}^s_{i,k} \times \mathbf{d}_{ij,k}}{||\mathbf{h}^s_{i,k} \times \mathbf{d}_{ij,k}||}, \tag{20}$$

and then to apply the Rodrigues' rotation formula to obtain $\mathbf{h}^s_{ideal,k}$ in the plan that contains both $\mathbf{d}_{ij,k}$ and $\mathbf{h}^s_{i,k}$ by rotating the baseline unit vector $\mathbf{h}^s_{ij,k}$ around $\mathbf{h}^s_{normal,k}$ by the angle θ_k according to the right hand rule:

$$\begin{aligned}\mathbf{h}^s_{ideal,k} &= \mathbf{h}^s_{ij,k}\cos(\theta_k) + (\mathbf{h}^s_{normal,k} \times \mathbf{h}^s_{ij,k})\sin(\theta_k) + \\ &\quad \mathbf{h}^s_{normal,k}(\mathbf{h}^s_{normal,k} \cdot \mathbf{h}^s_{ij,k})(1 - \cos(\theta_k)) \\ &= \mathbf{h}^s_{ij,k}\cos(\theta_k) + (\mathbf{h}^s_{normal,k} \times \mathbf{h}^s_{ij,k})\sin(\theta_k).\end{aligned} \tag{21}$$

Consequently, these newly defined unit steering vectors $\mathbf{h}^*_{i+j,k}$ and $\mathbf{h}^*_{ideal,k}$ for the differential LS problem can replace $\mathbf{h}^*_{i,k}$ in the $\mathbf{H}$ design matrix of (10) and (12). All the above described models will be compared to identify the best solution for GNSS ranging in space.

It has to be noticed that both users have an independent free clock. Therefore, the inter-user GNSS measurements are asynchronous with a timestamp offset $\Delta t_{ij,k}$ and have to be synchronized by using, for example, the range-rate information that can be inferred from the Doppler measurements.

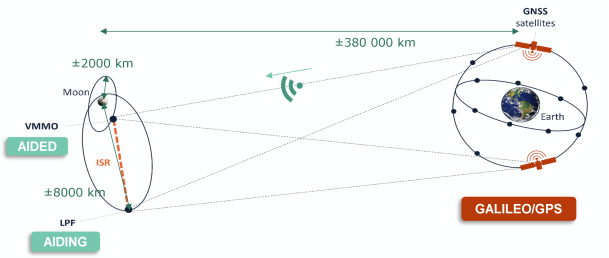

Fig. 2: Schematic of the GNSS scenario for VMMO and Pathfinder.

This aspect is of particular importance in the case of a space scenario involving orbiters, given the high users velocity.

The technique to synchronize the measurements of the aiding agent with the aided agent measurement timestamps is based on the Doppler frequency shift of the aiding agent j with the satellite s, $\phi^s_j(t_{j,k})$ so that

$$\begin{aligned}\hat{\rho}^s_j(t_{i,k}) &= \rho^s_j(t_{j,k} - \Delta t_{ij,k}) \\ &= \rho^s_j(t_{j,k}) - \Delta t_{ij,k} \cdot \lambda_{f_c} \cdot \phi^s_j(t_{j,k}),\end{aligned} \tag{22}$$

where λ_{f_c} is the wavelength associated to the carrier frequency of the GNSS signals, 0.2549 m for L5/E5a, being the focus frequency band of the present contribution, given its inherent advantages for spaceborne GNSS users, as discussed in [16]. In the present contribution however, in order to isolate the impact of the time-compensation quality on the ISR estimation process, the measurements of the aiding agent will be inferred at the aided agent timestamps with a shape-preserving piecewise cubic interpolation.

IV. The Considered Space Scenario

In order to analyze the applicability of the concept in space, a scenario including two lunar missions foreseen in the next years has been taken as a meaningful example. The estimation of the baseline length is performed between a lunar CubeSat, Volatile and Mineralogy Mapping Orbiter (VMMO), and the communication relay Lunar Pathfinder (LPF). A representative orbit for the VMMO mission consists in the Low Lunar Frozen Orbit (LLFO) of which the keplerian parameters are given in [17].

The second lunar mission considered in this paper, the LPF, will fly to the Moon in an Elliptical Lunar Frozen Orbit (ELFO). The goal of this mission is to serve as relay between lunar assets via the S-band and Earth in the X-Band [18]. The orbit of LPF favours a long duration coverage of the lunar southern hemisphere attractive for early lunar missions, and its orbital keplerian parameters are given in [19].

The overall scenario is depicted in Fig. 2. These two missions are realistic candidates to use DGNSS in space as they will both have a GNSS receiver aboard and a communication link to communicate with neighboring space missions. This

TABLE I: Comparison of the parallelism assumption validity between terrestrial and lunar scenarios.

Typical values	Terrestrial scenario	Lunar Scenario
Inter-agent distance (km)	[20; 200]	[2,500; 11,000]
User-to-satellite distance (km)	20,200	380,000
Validity ratio (‰)	[1; 10]	[5; 29]

scenario is simulated on the 09-Nov-2025 00:00:00.000 GPST when the presence in space of both user missions can be assumed.

To compare the parallelism assumption validity in a terrestrial scenario with respect to the space scenario of Fig.2., the ratio between the inter agents distance $d_{ij,k}$ and a typical user-to-satellite range $r^s_{*,k}$ is considered. The closer this ratio is to zero, the closer the assumption is to be valid. Table I presents typical values of this ratio in a terrestrial case with respect to the lunar scenario, considering the distances typical to the VMMO-Pathfinder cooperation and the Global Positioning System (GPS) constellation. The numbers shown in Table I show that in a DGNSS case applied to a typical lunar scenario, the ratio becomes significantly higher when compared to terrestrial applications. In the long-baseline DGNSS terrestrial applications presented in the literature, the dominant error factor becomes the ionospheric and tropospheric delays between the cooperating users such that the effect of the bias introduced by the assumption in (13) in the algorithm itself is not analyzed [20]–[22].

It has to be noted that the large spacecrafts velocity causes high pseudorange rates (values up to 20 kHz in terms of Doppler shift vs 2 kHz for terrestrial ground users) as well as making the baseline length variation rate to be significantly large.

V. Methodology

To assess the performances of GNSS ranging based on the measurements made by a real spaceborne receiver in lunar orbit, the three segments of a GNSS positioning scenario followed by a post-processing phase are emulated.

A. User segment

The user segment made up of the NaviMoon receiver is then set up to run an aided GNSS scenario fed with an RF cable from the Radio Frequency Constellation Simulator (RFCS) generated signals. An Engineering Model version of the receiver is in the Radio Navigation Laboratory of ESA and it was used to perform the present tests. The NaviMoon receiver is a high-sensitivity spaceborne receiver with an acquisition engine sensitivity as low as 18 dB-Hz and a tracking threshold of 15 dB-Hz on L1/E1 and 12 dB-Hz on L5/E5a [23]. Aided data can be provided to the receiver to search only visible satellites, predict Doppler and prioritise satellites with high C/N_0.

The receiver antenna pattern is an omnidirectional pattern with a 0 dB antenna gain. The necessary power gain to complete the link budget to meet a descent visibility is set on the system side. It is assumed that this would not cause a significant difference in the performances with respect to the real scenario given the fact that the intended high-gain 14 dBi Harp antenna will be steerable and have a relatively flat antenna gain over the beamwith covering the Earth GNSS satellites directions as seen by the lunar orbiter [23].

B. Space segment and Control segment

The space segment of the present scenario includes a high-fidelity orbit propagator to generate the reference trajectories of the VMMO and of the LPF. These ground truths are then injected in a GNSS RFCS to create representative signals for a user in lunar orbit. The space segment of the simulated scenario is run by the ESA Radio Navigation Laboratory's RFCS. The considered GPS constellation consists of 32 satellites. No tropospheric nor ionospheric errors was applied since the percentage of Earth GNSS signals acquired at the Moon that passes through the Earth's atmosphere is actually negligible. The GNSS antenna patterns used for this specific scenario are flat with a transmission gain of 5 dB and an additional 10 dB global offset has been applied to the entire constellation. Furthermore, an additional gain has been applied to compensate for the absence of receiver antenna pattern as mentioned in section V-A. This additional gain was selected based on a previously run STK scenario to match the carrier to noise density ratio levels representative of a lunar scenario.

The control segment communicates with the NaviMoon receiver using Telemetry and Telecommand (TM/TC) to provide the receiver with the necessary aiding and to retrieve and store the GNSS observables measurements. Finally, the post-processing block runs a positioning algorithm based on the receiver raw measurements logs and tests the various GNSS ranging techniques.

VI. Results

For the purpose of comparing the ISR estimation performances with the already known ones on Earth, a terrestrial scenario is also presented here below. It is made of two GNSS ground static users with a fixed baseline of 1 km.

Fig. 3 shows the GNSS visibility of the aided agent as well as the number of satellites commonly visible to both users, named "shared", which will be used for the differential GNSS ranging techniques, for the terrestrial and lunar scenario, respectively. It shows that the number of satellites usable for the differential ranging techniques drop from 10-12 for Earth ground users to 0-7 for a lunar scenario. On top of the lower signals power received by the Moon receiver, the lunar missions also suffer from periodical obstruction from the Moon's limb.

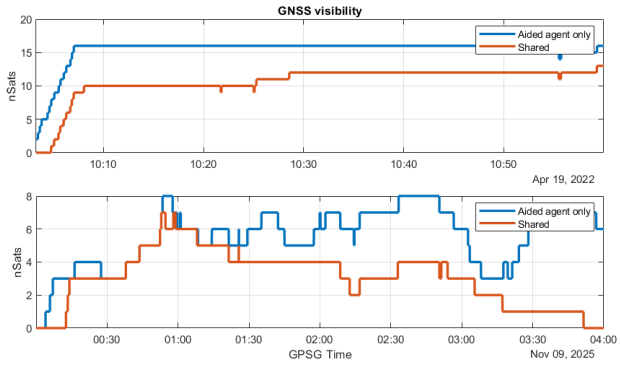

Fig. 3: GNSS Visibility for a terrestrial scenario (top) and a lunar scenario (bottom).

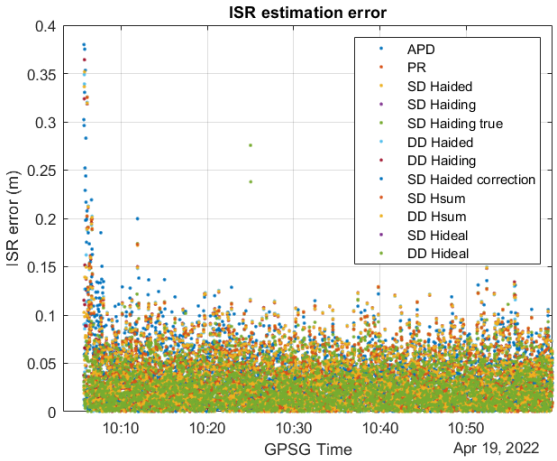

Fig. 4: ISR estimation error over time for a terrestrial scenario using interpolated aiding pseudoranges.

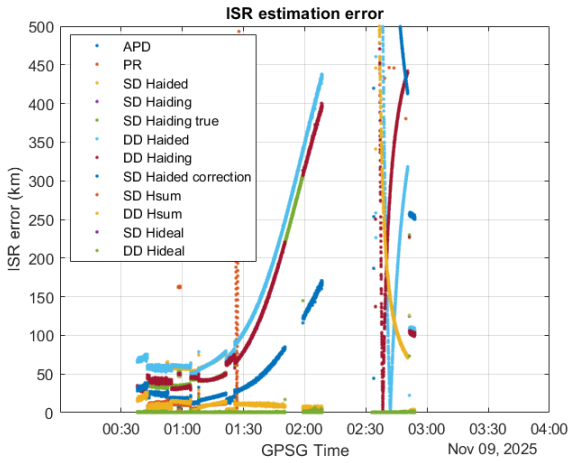

Fig. 5: ISR estimation error over time for a lunar scenario using interpolated aiding pseudoranges.

TABLE II: ISR error statistics: comparison table.

ISR error Statistics	**Terrestrial static case (m)** $75^{th}perc$	**Lunar dynamic case (km)** $75^{th}perc$
APD	0.037	0.599
PR	0.045	1E13
SD Haided	0.045	251.748
SD Haiding	0.045	208.427
SD Haiding true	0.045	261.06
DD Haided	0.047	251.748
DD Haiding	0.047	208.427
SD Haided correction	0.049	142.85
SD Hsum	0.045	12.228
DD Hsum	0.047	14.357
SD Hideal	0.037	0.599
DD Hideal	0.037	0.599

A. ISR estimation error comparison

The ISR estimation error over time and in terms of statistics is also discussed for both the terrestrial scenario and the lunar scenario, for all the techniques presented in the Section II. The legend of the graphs for the ISR estimation error indicates the name of the ISR estimation techniques depending on the design matrix $\mathbf{H}$ and the chosen unit steering vector. For example, the technique **SD Haided** corresponds to the SD technique with the design matrix made of the unit steering vectors originating in the aided agent estimated position. The technique **SD Haiding true** corresponds to the SD technique with the steering vectors originating in the true position of the aiding agent. This is done to understand the impact of the quality of the position estimate used in the design matrix on the final ISR estimation error. The technique **SD Haided correction** corresponds to the SD technique where the bias introduced by the parallelism assumption was corrected according to (15). The technique **SD Hsum** corresponds to the SD technique with the design matrix made of the unit steering vectors defined in (16). Fig. 4 shows that, as expected for a terrestrial scenario, the ISR estimators presented above behave as unbiased estimators, hence validating the parallelism assumption considered for ground applications. Table II showing the 75th percentile of the ISR error displays therefore a low variability between the different techniques in terms of performances, at sub-decimeter level for a static ground scenario. When moving to a lunar scenario, as depicted in Fig. 5, the situation is completely different. The error becomes very dependent on the ISR ground truth, slowing increasing up to 02:40, where it reaches its peak value. A few algorithms however seem to behave independently of the ISR truth, namely SD Hsum, DD Hsum, SD Hideal, DD Hideal and APD, as emphasized by the numbers in table II.

VII. CONCLUSION

The present contribution shows the potential of differential GNSS techniques for a lunar scenario of cooperating users. The results showed that the commonly used algorithms for Earth are not applicable directly to space and some modifications to the design matrix allowed to reduce the dependency of the ISR estimation error in the actual baseline length. It must be kept in mind that the presented performances are a lower limit case as the common number of visible satellites

involved in the GNSS ranging algorithms is very low and this could be improved with higher user antenna gains or with a focus on simulation periods where the users do not suffer from the Moon's limb obstruction.

ACKNOWLEDGMENTS

This work has been performed under the ESA Contract No. 4000134565/21/NL/GLC/my that is co-funding the PhD grant of Ms. Anaïs Delépaut. The content of the present article reflects solely the authors' view and by no means represents the official view of the European Space Agency (ESA). In any reproduction of this article, there should not be any suggestion that ESA or this article endorses any specific organisation or products. The use of the ESA logo is not permitted. This notice should be preserved along with the article's original URL.

REFERENCES

[1] ESA, "Moonlight: connecting earth with the moon," https://www.esa.int/ESA_Multimedia/Videos/2020/11/Moonlight_connecting_Earth_with_the_Moon, 2021.

[2] P. Giordano, A. Grenier, P. Zoccarato, R. Swinden, D. Trenta, E. Schoenemann, F. Liucci, W. Enderle, B. Hufenbach, and J. Ventura-Traveset, "Orbit determination and time synchronisation in lunar orbit with gnss-lunar pathfinder experiment," in *IAC 2021 Congress Proceedings, 72nd International Astronautical Congress*, 2021.

[3] J. J. Parker, F. Dovis, B. Anderson, L. Ansalone, B. Ashman, F. H. Bauer, G. D'Amore, C. Facchinetti, S. Fantinato, G. Impresario *et al.*, "The lunar gnss receiver experiment (lugre)," in *Proceedings of the 2022 International Technical Meeting of The Institute of Navigation*, 2022, pp. 420–437.

[4] M. Tahir, S. S. Afzal, M. S. Chughtai, and K. Ali, "On the accuracy of inter-vehicular range measurements using GNSS observables in a cooperative framework," *IEEE Transactions on Intelligent Transportation Systems*, pp. 1–10, Jun. 2018.

[5] K. Liu, H. B. Lim, E. Frazzoli, H. Ji, and V. C. S. Lee, "Improving positioning accuracy using GPS pseudorange measurements for cooperative vehicular localization," *IEEE Transactions on Vehicular Technology*, vol. 63, no. 6, pp. 2544–2556, Jul. 2014.

[6] A. Minetto, M. C. Bello, and F. Dovis, "Dgnss cooperative positioning in mobile smart devices: A proof of concept," pp. 3480–3494, 2022.

[7] D. Gu, B. Ju, J. Liu, and J. Tu, "Enhanced GPS-based GRACE baseline determination by using a new strategy for ambiguity resolution and relative phase center variation corrections," *Acta Astronautica*, vol. 138, pp. 176–184, Sep. 2017.

[8] P. Chen, L. Shu, R. Ding, and C. Han, "Kinematic single-frequency relative positioning for LEO formation flying mission," *GPS Solut.*, vol. 19, no. 4, p. 525–535, oct 2015. [Online]. Available: https://doi.org/10.1007/s10291-014-0410-8

[9] G. Allende-Alba and O. Montenbruck, "Robust and precise baseline determination of distributed spacecraft in leo," *Advances in Space Research*, vol. 57, no. 1, pp. 46–63, 2016. [Online]. Available: https://www.sciencedirect.com/science/article/pii/S027311771500695X

[10] P. Giordano, F. Malman, R. Swinden, P. Zoccarato, and J. Ventura-Traveset, "The lunar pathfinder pnt experiment and moonlight navigation service: The future of lunar position, navigation and timing," in *Proceedings of the 2022 International Technical Meeting of The Institute of Navigation*, 2022, pp. 632–642.

[11] N. Gogoi, A. Minetto, and F. Dovis, "On the cooperative ranging between android smartphones sharing raw GNSS measurements," in *2019 IEEE 90th Vehicular Technology Conference (VTC2019-Fall)*, 2019, pp. 1–5.

[12] B. Hofmann-Wellenhof and J. C. H. Lichtenegger, *Global positioning system: theory and practice*. Springer Science & Business Media, 2012.

[13] E. D. Kaplan and C. Hegarty, *Understanding GPS/GNSS: principles and applications*. Artech House, 2017.

[14] D. Yang, F. Zhao, K. Liu, H. B. Lim, E. Frazzoli, and D. Rus, "A gps pseudorange based cooperative vehicular distance measurement technique," in *2012 IEEE 75th Vehicular Technology Conference (VTC Spring)*. IEEE, 2012, pp. 1–5.

[15] N. Wu, H. Qin, and C. Zhao, "Long-baseline differential doppler positioning using space-based sop based on bpvgmm," *IEEE Transactions on Instrumentation and Measurement*, 2023.

[16] A. Delépaut, P. Giordano, J. Ventura-Traveset, D. Blonski, M. Schönfeldt, P. Schoonejans, S. Aziz, and R. Walker, "Use of gnss for lunar missions and plans for lunar in-orbit development," *Advances in Space Research*, vol. 66, no. 12, pp. 2739–2756, 2020.

[17] S. Rowe, R. Kruzelecky, P. Murzionak, I. Sinclair, M. Corriveau, R. Walker, J. Vennekens, Y. Gao, C. Bridges, N. Baresi *et al.*, "Lunar volatile and mineralogy mapping orbiter (vmmo): Viable science from lunar cubesats," 2021.

[18] SURREY, "Lunar pathfinder," https://www.sstl.co.uk/space-portfolio/missions-in-build/2021/lunar-pathfinder, 2021.

[19] S. S. T. Ltd, "Lunar pathfinder data relay satellite in orbit around the moon," https://www.sstl.co.uk/getmedia/690f1da3-a935-4c4d-b48c-616ac8417cb1/LunarPathfinder-UserManual-WebSite-v003.pdf, 2020.

[20] B. Bramanto, I. Gumilar, M. Taufik, and I. M. D. Hermawan, "Long-range single baseline RTK GNSS positioning for land cadastral survey mapping," in *E3S Web of Conferences*, vol. 94. EDP Sciences, 2019, p. 01022.

[21] I. Gumilar, B. Bramanto, F. F. Rahman, and I. M. D. Hermawan, "Variability and performance of short to long-range single baseline RTK GNSS positioning in indonesia," in *E3S Web of Conferences*, vol. 94. EDP Sciences, 2019, p. 01012.

[22] V. Giralo and S. D'Amico, "Precise real-time relative orbit determination for large-baseline formations using GNSS," in *Proceedings of the 2021 International Technical Meeting of The Institute of Navigation*, 2021, pp. 366–384.

[23] NAVISP, "How to navigate on the moon?" https://navisp.esa.int/news/article/How%20to%20navigate%20on%20the%20moon%3F, 2023.